



Fabrication of Cu⁰-composited CuFe₂O₄ magnetic nanoparticles on diatomite support for efficient degradation of tetracycline hydrochloride by a Fenton-like system

Shuai Deng^a, Zhi Guo^b, Yi-Han Chen^b, Kang-Ping Cui^b, Zhao-Gang Ding^b, Bei Wang^c, Rohan Weerasooriya^{a,d}, Xing Chen^{a,b,d,*}

^a Key Lab of Aerospace Structural Parts Forming Technology and Equipment of Anhui Province, Institute of Industry and Equipment Technology, Hefei University of Technology, Hefei 230009, PR China

^b Key Laboratory of Nanominerals and Pollution Control of Higher Education Institutes, School of Resources and Environmental Engineering, Hefei University of Technology, Hefei 230009, PR China

^c Anqing Changhong Chemical Co., Ltd., Anqing 246002, PR China

^d National Centre for Water Quality Research, National Institute of Fundamental Studies, Hantana, Kandy, Sri Lanka

ARTICLE INFO

Editor: Luigi Rizzo

Keywords:

CuFe₂O₄
Copper
Diatomite
Fenton-like reaction
Tetracycline hydrochloride

ABSTRACT

Paramagnetic Cu/CuFe₂O₄/DE composites were fabricated by a one-step solvothermal method to design a heterogeneous Fenton-like catalyst to degrade tetracycline hydrochloride (TC). The Cu/CuFe₂O₄/DE were characterized by SEM, TEM, XRD, BET, and XPS methods. The catalytic activity of CuFe₂O₄ was improved using diatomite and Cu⁰. Diatomite (DE) enhanced the dispersity of Cu/CuFe₂O₄, minimized metal ions leaching, and improved stability. The Cu⁰ is used for the regeneration of Fe³⁺. The synergy between Cu⁺/Cu²⁺ and Fe²⁺/Fe³⁺ redox pairs promotes hydroxyl radical production upon H₂O₂ decomposition. The synthesized materials were characterized by SEM, TEM, XRD, BET, and XPS, and their catalytic activities were discussed and analyzed. 95.5 % TC was degraded within 90 min (initial conditions, pH = 5.0 and [TC] 50 mg/L), and showing excellent anti-interference ability to the presence of SO₄²⁻, Cl⁻, NO₃⁻, CO₃²⁻ and humic acid (HA). The presence of active species, viz., •OH and •O₂ radicals generated in the Cu/CuFe₂O₄/DE/H₂O₂ system were detected by ESR quenching measurements. The •OH and •O₂ mediated TC degraded pathways were proposed using the intermediates identified by LC-MS data. The novel heterogeneous Fenton-like process developed using Cu/CuFe₂O₄/DE/H₂O₂ is robust for TC degradation as exemplified in its stability and reusability measurements.

1. Introduction

Antibiotics are widely used in medicine, animal husbandry, and agriculture posing a serious threat of their wastes to the environment [1]. Tetracycline (TC) is a widely used antibiotic in medical treatment and animal husbandry. It is persistent and stable under natural environmental conditions with a long half-life [2,3]. TC weakly absorbs by living organisms thus emanating it readily through wastes creating serious implications for ecosystem health [4–6]. In recent years, TC is frequently detected in surface water, drinking water, and soils at elevated proportions [7,8]. Although relatively low concentrations of TC are detected in the natural aqueous environment (µg/L–ng/L), high concentrations (100–500 mg/L) are detected in effluents of hospital and

pharmaceutical industries [9,10]. Therefore, the development of novel methods to remediate TC-polluted wastewater is a pressing global need.

Presently, TC in water is treated using adsorption [11], membrane separation [12], biodegradation [13], photocatalysis [14], and advanced oxidation processes [15]. Both adsorption and membrane separation methods concentrate TC without really destroying them. Biodegradation methods sometimes are not efficient to treat TC due to their microbial resistance [16]. Photocatalysis techniques are costly and time intensive especially in treating TC-laden wastewater [17]. When compared to these methods, the advanced oxidation processes (AOPs) are efficient as they completely destruct antibiotics via non-selective free radicals generated in different routes [18–20]. Among them, Fe²⁺/Fe³⁺ in the traditional Fenton process can activate H₂O₂ to

* Corresponding author at: Key Lab of Aerospace Structural Parts Forming Technology and Equipment of Anhui Province, Institute of Industry and Equipment Technology, Hefei University of Technology, Hefei 230009, PR China.

E-mail address: xingchen@hfut.edu.cn (X. Chen).

<https://doi.org/10.1016/j.jece.2023.110045>

Received 30 January 2023; Received in revised form 25 April 2023; Accepted 2 May 2023

Available online 3 May 2023

2213-3437/© 2023 Elsevier Ltd. All rights reserved.

generate highly reactive $\bullet\text{OH}$ destruct antibiotics into benign products [21]. Homogeneous Fenton oxidation has disadvantages such as slow reaction, narrow operational pH window [22], and excess iron-containing sludge production [23]. However, the heterogeneous Fenton-like processes can overcome these shortcomings; they have the advantages of simple operation, high efficiency, low cost, and less sludge production [24]. In heterogeneous Fenton-like catalysts, the presence of iron-containing compounds is mandatory. CuFe_2O_4 with spinel structure is a P-type semiconductor material with a narrow band gap of 1.4 eV, which can respond under visible light without photo-corrosion [25]. CuFe_2O_4 is chemically stable, environmentally benign, and easily recoverable under a magnetic flux. However, it has some inherent limitations such as sluggish electrons transfer for $\text{Fe}^{3+} \rightarrow \text{Fe}^{2+}$ conversion and easy particulates agglomeration.

Several zero-valent metals (Fe^0 , Al^0 , and Cu^0) are commonly employed for the degradation of organic pollutants in water [26–28]. Cu^0 activates H_2O_2 for $\bullet\text{OH}$ production to degrade organic pollutants, mainly through the $\text{Cu}^{2+}/\text{Cu}^+$ catalytic reduction cycle under acidic conditions [29]. Zhou et al. [30] found complete degradation of p-benzoic acid within 25 min in the $\text{Cu}^0/\text{H}_2\text{O}_2$ system at pH 3.0. Cu^0 undergoes uncontrolled oxidation in water irrespective of the presence of organic pollutants in the system. However, they passivate after repeated use. Mixed valence metals offer an alternative solution for the destruction of organic pollutants. The reactivity of $\text{Cu}^0/\text{Fe}_3\text{O}_4$ nanocomposite is enhanced enabling the destruction of 4-chlorophenol into harmless products, and the degradation efficiency is 10.9 times or 7.3 times higher than that of employing discrete Cu^0 or Fe_3O_4 nanoparticles [31]. Therefore, the catalytic performance of CuFe_2O_4 can be enhanced by introducing Cu^0 into the composite.

To minimize catalyst agglomeration, materials with uniform void structures and large specific surface areas, such as diatomite [32], polystyrene [33], chitosan [34] and polymeric filter materials [35] are chosen as the carriers. Diatomite is a SiO_2 polymorph around 10–50 μm size range found in natural environments. It has high porosity, high specific surface area, lightweight, strong adsorption capacity, and high chemical stability. In diatomite shells, silicon hydroxyl sites abut from the surface can capture metal ions readily thus inhibiting catalyst leaching. Therefore, diatomite is an ideal carrier to retain a catalyst in a well-dispersed manner with minimal metal ions leaching [36]. Zhu et al. [37] prepared Ag_3PO_4 /diatomite composites with photocatalytic efficiency four-fold higher than that of pure Ag_3PO_4 . due to the efficient separation of photogenerated electron-hole pairs. Tan et al. [32] synthesized porous magnetic catalyst CoFe_2O_4 /diatomite (CFD) by citrate combustion method. The high surface area, better crystal dispersion, and abundant active sites make CFD better than CoFe_2O_4 for the degradation of bisphenol A (BPA). The pseudo-first-order reaction rate constant of $\text{CoFe}_2\text{O}_4/\text{DE}$ is over five times higher than that of pure CoFe_2O_4 . Therefore, the introduction of diatomite can reduce the particulates' agglomeration providing free active sites to improve the catalytic activity and stability.

Presently, we fabricated $\text{Cu}/\text{CuFe}_2\text{O}_4/\text{DE}$ and associated composites by a one-step solvothermal method, and their performance was examined for the degradation of TC via a heterogeneous Fenton-like process. The effect of solution pH, matrix ions, and humic acid on the efficiency of TC degradation was also assessed. The mechanistic pathways of TC degradation were elucidated by LC-MS and electron spin resonance spectroscopic methods. The sustainability of the $\text{Cu}/\text{CuFe}_2\text{O}_4/\text{DE}$ Fenton-like process was also examined by mimicking real-world experiments.

2. Experiments

2.1. Materials and chemicals

Diatomite was purchased from International Building Materials Environmental Protection Technology Co., Ltd PR China. Ferric chloride

hexahydrate ($\text{FeCl}_3\bullet 6\text{H}_2\text{O}$), copper chloride dihydrate ($\text{CuCl}_2\bullet 2\text{H}_2\text{O}$), sodium acetate (CH_3COONa), and ethylene glycol (EG) were purchased from Sinopharm Chemical Reagent Co., Ltd, PR China. Polyethylene glycol (PEG2000), hydrochloric acid (HCl), sodium hydroxide (NaOH), tert-butanol (TBA), p-benzoquinone (BQ), and tetracycline hydrochloride (TC) were purchased from Shanghai McLean Chemical Co., Ltd, PR China. The analytical grade chemical reagents and deionized water were used as received in all experiments.

2.2. Synthesis of $\text{Cu}/\text{CuFe}_2\text{O}_4/\text{DE}$ and allied composites

$\text{Cu}/\text{CuFe}_2\text{O}_4/\text{DE}$ composites were synthesized by a one-step solvothermal method. Firstly, 0.5 g diatomite was dispersed in 30 ml of ethylene glycol, and then 1.6 mmol $\text{CuCl}_2\bullet 2\text{H}_2\text{O}$ and 3.2 mmol $\text{FeCl}_3\bullet 6\text{H}_2\text{O}$ were co-dispersed in 30 ml of ethylene glycol. While stirring, the $\text{CuCl}_2\bullet 2\text{H}_2\text{O}$ and $\text{FeCl}_3\bullet 6\text{H}_2\text{O}$ solutions were added dropwise to the diatomite suspension, and then 0.75 g polyethylene glycol and 2.0 g sodium acetate were added respectively to form a homogeneous green solution. The uniform green solution thus received was loaded into 100 ml polytetrafluoroethylene lining and autoclaved at 200 °C for 12 h. After cooling to room temperature, the precipitate was magnetically separated, washed three times with absolute ethanol and deionized water, and vacuum dried at 60 °C for 10 h. (The molar ratio of Cu^0 , CuFe_2O_4 , and diatomite is approximately 1.008:1:10.320). The synthesis of $\text{Cu}/\text{CuFe}_2\text{O}_4$, Cu^0 and Cu/DE catalysts was prepared as described above without adding diatomite and $\text{FeCl}_3\bullet 6\text{H}_2\text{O}$, respectively. CuFe_2O_4 and $\text{CuFe}_2\text{O}_4/\text{DE}$ were obtained by oxidizing Cu^0 in $\text{Cu}/\text{CuFe}_2\text{O}_4$ and $\text{Cu}/\text{CuFe}_2\text{O}_4/\text{DE}$ nanocomposites using FeCl_3 aqueous solution. The term catalyst implied either of the following substrates; $\text{Cu}/\text{CuFe}_2\text{O}_4/\text{DE}$, $\text{CuFe}_2\text{O}_4/\text{DE}$, $\text{Cu}/\text{CuFe}_2\text{O}_4$, CuFe_2O_4 , or Cu/DE .

2.3. Catalyst characterization

The crystalline phase and purity of the fabricated substrates were tested using a rotating target X-ray diffractometer (XRD, Rigaku, Japan). The microscopic morphology, structure, and elemental composition were analyzed by scanning electron (SEM, Hitachi, Japan) and transmission electron (HRTEM, JEOL, Japan) microscopy equipped with X-ray energy dispersive spectrometer (EDS). The surface functional groups of the samples were analyzed by Fourier transform infrared spectrometer (Thermo Nicolet, USA). The surface chemical properties of the materials and the changes in the valence of the elements before and after the experiments were studied by X-ray photoelectron spectroscopy (XPS, Thermo, USA). The specific surface area and pore size distribution of the samples were investigated by a BET analyzer (Autosorb-IQ3, USA). The concentration of metal ions during the reaction was measured by an atomic absorption spectrometer (AA800, Perkin Elmer, USA).

2.4. TC degradation

A typical TC degradation experiment was carried out in batch mode in the dark. 10 mg catalyst was added to 50 ml (50 mg/L) TC aqueous solution, and the initial pH was adjusted with 0.1 M HCl or 0.1 M NaOH, under stirring. The catalyst was added for 30 min to ensure that the sample reached adsorption-desorption equilibrium, and then a pre-defined concentration of H_2O_2 is added. At given time intervals, 1.0 ml of the reaction solution was taken out and the catalyst was filtered with a 0.45 μm polyether sulfone membrane filter, followed by the addition of 0.5 ml of methanol as a quencher to stop the reaction. To determine the reusability of the catalyst, the used catalyst was collected, washed, and dried for use in subsequent experiments.

2.5. Analytical methods

The concentration of TC was measured by liquid chromatography using a C18 column (4.6 \times 250 mm) through a high-performance liquid

chromatograph (LC, Shimadzu LC-20A, Japan) and a UV detector with a wavelength of 355 nm. The mobile phase consisted of 20 % acetonitrile and 80 % 10 mM oxalic acid solution at a flow rate of 1.0 ml/min. Analysis of total organic carbon (TOC) was carried out using a TOC analyzer (multi-N/c3100, Germany) to evaluate the mineralization rate of TC. Electron spin resonance spectroscopy (ESR, Bruker, Germany) was used to detect the reactive radicals generated during the reaction. The Specific electronic spin resonance spectroscopy (ESR) analysis procedures are in [supporting Materials](#) text 1. The degradation intermediates generated during TC degradation were determined and analyzed by a liquid chromatogram-time-of-flight mass spectrometer (ACQUITY UPLC LCT Premier XE, USA) to explore the possible degradation routes.

3. Results and discussion

3.1. Characterization of the as-synthesized catalysts

As shown in [Fig. 1](#), the morphology and microstructure of diatomite (DE), Cu/CuFe₂O₄, and Cu/CuFe₂O₄/DE composites were examined by high-resolution field emission scanning electron microscopy (FESEM). FESEM analysis shows that the particle sizes of individual diatomite range from 10 μm to 50 μm. The disc shape diatomite surface shows a large array of pores that offers ideal locations to adhere Cu/CuFe₂O₄. In the absence of diatomite, Cu/CuFe₂O₄ nanocomposites readily agglomerate ([Fig. 1.b](#)). As shown in [Fig. 1\(a\)](#), a large number of pores are distributed on the surface of disc-shaped diatomite, and they provide housing for Cu/CuFe₂O₄ minimizing particulates agglomeration. Some Cu/CuFe₂O₄/DE particulates entered into the pores improving the dispersion ([Fig. 1.c](#)). Well-resolved Cu/CuFe₂O₄-impregnated diatomite (Cu/CuFe₂O₄/DE) provides enhanced catalytic reactivity. As shown in [Fig. 1](#). (d), Cu, Fe, O, and Si on Cu/CuFe₂O₄/DE show homogeneous distribution which further confirms Cu/CuFe₂O₄ adherence on diatomite with some uniformity.

Further structural details and elements distribution of Cu/CuFe₂O₄/DE samples were examined by transmission electron microscopy (TEM) and selected area electron diffraction (SAED). As shown in [Fig. 2\(a\)](#) and (b) Cu/CuFe₂O₄ is evenly dispersed on the surface and in the pores of diatomite, [Fig. 3\(c\)](#) is the HRTEM image of Cu/CuFe₂O₄/DE, which clearly shows some fringes with a lattice spacing of 0.25 nm, 0.29 nm, and 0.48 nm correspond to the (311), (220) and (111) crystal planes of CuFe₂O₄ respectively [38]. The lattice spacing of 0.21 nm matches the (111) crystal plane of Cu⁰ [39]. Five diffraction rings can be observed in [Fig. 2\(d\)](#) of the selected electron diffraction pattern of Cu/CuFe₂O₄/DE, also corresponding to the typical crystal plane of CuFe₂O₄ [40,41]. Therefore, HRTEM and SAED images further confirmed that the Cu/CuFe₂O₄/DE composite was successfully synthesized.

The crystal structure and crystallinity of diatomite, Cu/CuFe₂O₄, and Cu/CuFe₂O₄/DE were investigated by X-ray diffraction. As shown in [Fig. 3\(a\)](#), the diffraction peaks of Cu/CuFe₂O₄/DE located at 2θ = 18.3°, 30.2°, 35.5°, 37.2°, 43.2°, 53.6°, 57.1°, 62.7°, and 74.2° correspond to (111), (220), (311), (222), (400), (422), (511), (400) and (533) crystal planes of CuFe₂O₄ respectively (JCPDS : 77-0010). In addition, the diffraction peaks detected at 2θ = 43.3°, 50.4° and 74.1° correspond to the (111), (200), and (220) crystal planes of Cu⁰ (JCPDS : 85-1326). The diffraction peak of diatomite around 2θ = 26.6° corresponds to the (101) crystal plane of SiO₂ (JCPDS : 46-1045) [42]. The Scherrer formula was used to calculate the grain size of Cu⁰ and CuFe₂O₄. The average grain size of Cu⁰ and CuFe₂O₄ in Cu/CuFe₂O₄/DE was 32.761 nm and 13.457 nm, which is smaller than that of pure Cu⁰ (43.832 nm) and CuFe₂O₄ (22.981 nm). The diffraction patterns of Cu/CuFe₂O₄/DE samples combine the characteristic diffraction peaks of Cu, CuFe₂O₄, and diatomite. The spectral data further confirms the successful fabrication of CuFe₂O₄ on diatomite (designated as Cu/CuFe₂O₄/DE).

[Fig. 3\(b\)](#) displays the FT-IR spectra of diatomite, Cu/CuFe₂O₄, and Cu/CuFe₂O₄/DE composites. The IR bands of Cu/CuFe₂O₄ at 451.70 cm⁻¹ and 578.93 cm⁻¹ correspond to Cu-O and Fe-O stretching vibrations [43], respectively. The IR bands at 465.66 cm⁻¹ and 1093.57 cm⁻¹ are due to the asymmetric stretching vibration of Si-O-Si, and the band at 796.44 cm⁻¹ is attributed to the bending vibrations of Si-O-Al in diatomite [44]. The Al may associate as an impurity in diatomite. In addition, the IR bands at 1632.01 cm⁻¹ and 3436.02 cm⁻¹ correspond to the bending and stretching vibrations of H-O-H and -OH adsorbed water on diatomite, respectively [45].

Diatomite is an ideal carrier for catalysts due to its unique porous structure. As shown in [Fig. 4\(a\)](#), the N₂ adsorption-desorption curves of Cu/CuFe₂O₄/DE and DE both follow a typical IV curve, showing the H3 hysteresis loop, indicating a mesoporous structure. This structure is conducive to the enrichment and diffusion of pollutants into the active centers of the catalyst improving its efficiency [32]. The specific surface areas and pore sizes of Cu/CuFe₂O₄, Cu/CuFe₂O₄/DE, and diatomite are (11.6 m²g⁻¹, 57.2 m²g⁻¹, and 20.1 m²g⁻¹) and (3.78 nm, 4.89 nm, and 6.08 nm), respectively. Compared with diatomite without a catalyst, Cu/CuFe₂O₄/DE has a larger specific surface area and narrower pore size, which determines that Cu/CuFe₂O₄/DE has better adsorption and catalytic activity.

[Fig. 5](#) shows the XPS survey spectrums for pristine and Cu/CuFe₂O₄/DE after TC degradation by a Fenton-like process (viz. hereafter spent Cu/CuFe₂O₄/DE). The XPS survey spectrums show the presence of five elements ([Fig. S1](#)), namely Cu, O, Si, and C in both composites, viz. pristine and spent Cu/CuFe₂O₄/DE. The presence of surface-derived C is ascribed to the carbonization of ethylene glycol used as a solvent and the hydrocarbons present in the ambient air [46,47]. Fine spectral

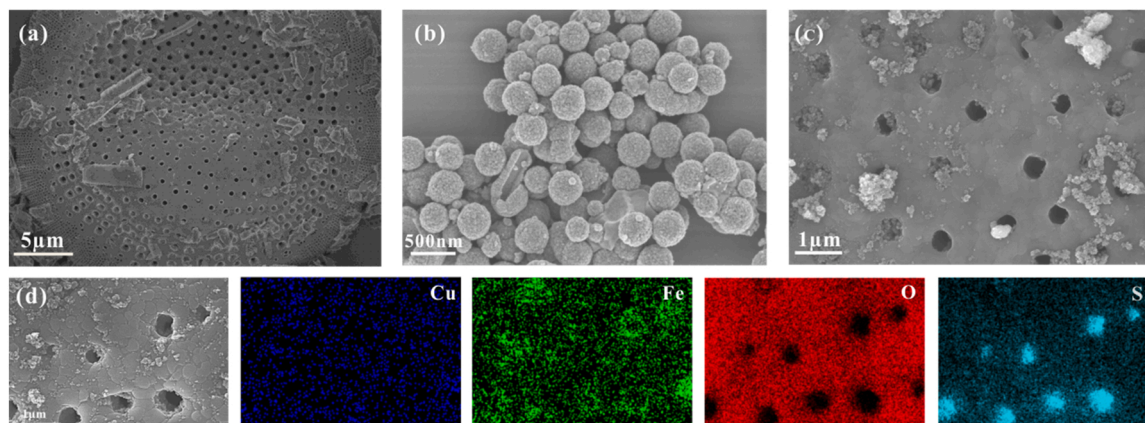


Fig. 1. FESEM images of (a) diatomite, (b) Cu/CuFe₂O₄(c) Cu/CuFe₂O₄/DE composite, (d) Element mapping of Cu/CuFe₂O₄/DE composite.

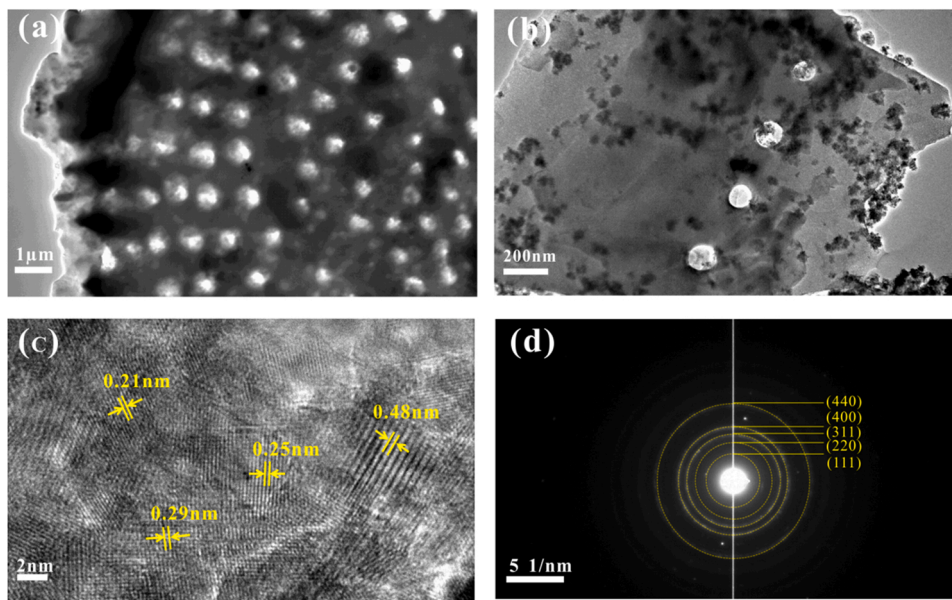


Fig. 2. TEM image (a) and (b), HRTEM image (c), and SAED pattern (d) of Cu/CuFe₂O₄/DE composite.

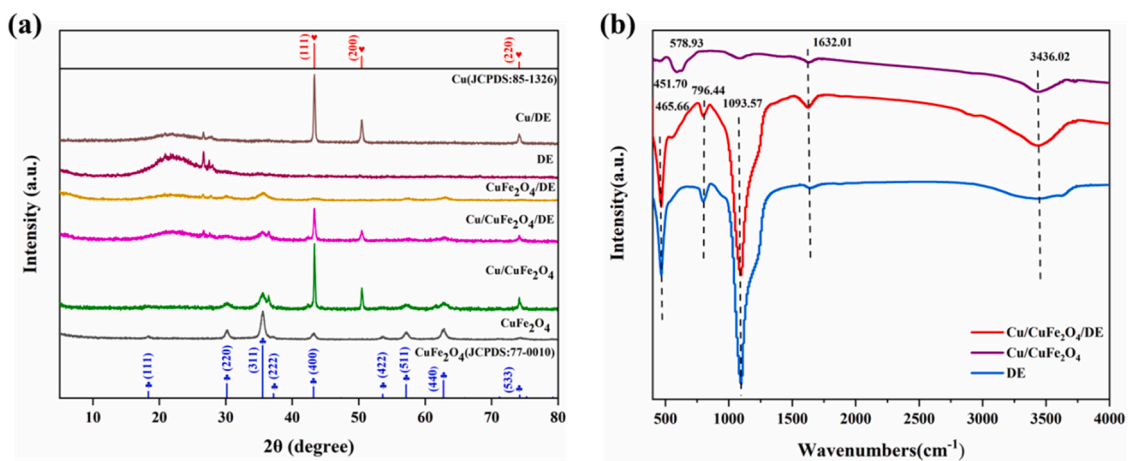


Fig. 3. The XRD patterns (a) and FT-IR spectra (b) of synthesized catalysts.

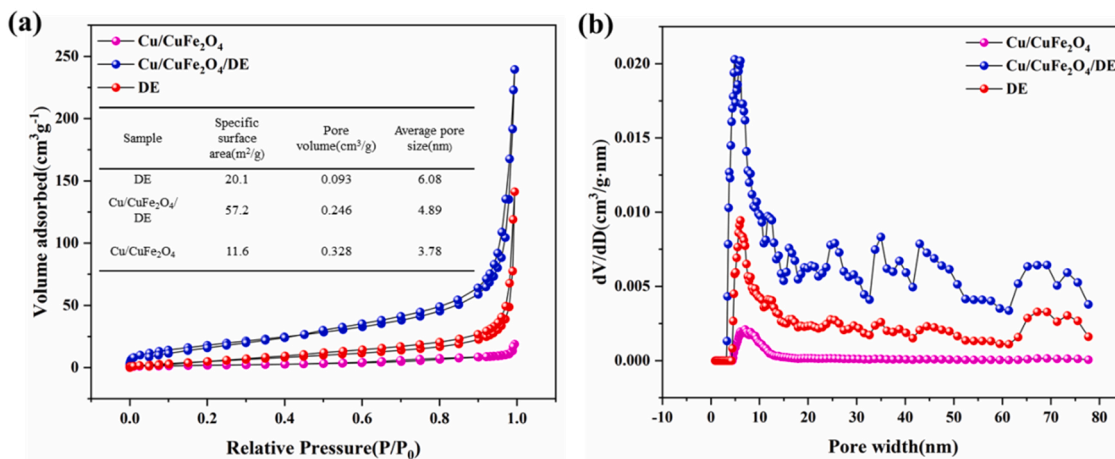


Fig. 4. N₂ adsorption-desorption isotherms (a) and pore size distribution plots (b) of Cu/CuFe₂O₄, diatomite, and Cu/CuFe₂O₄/DE composite.

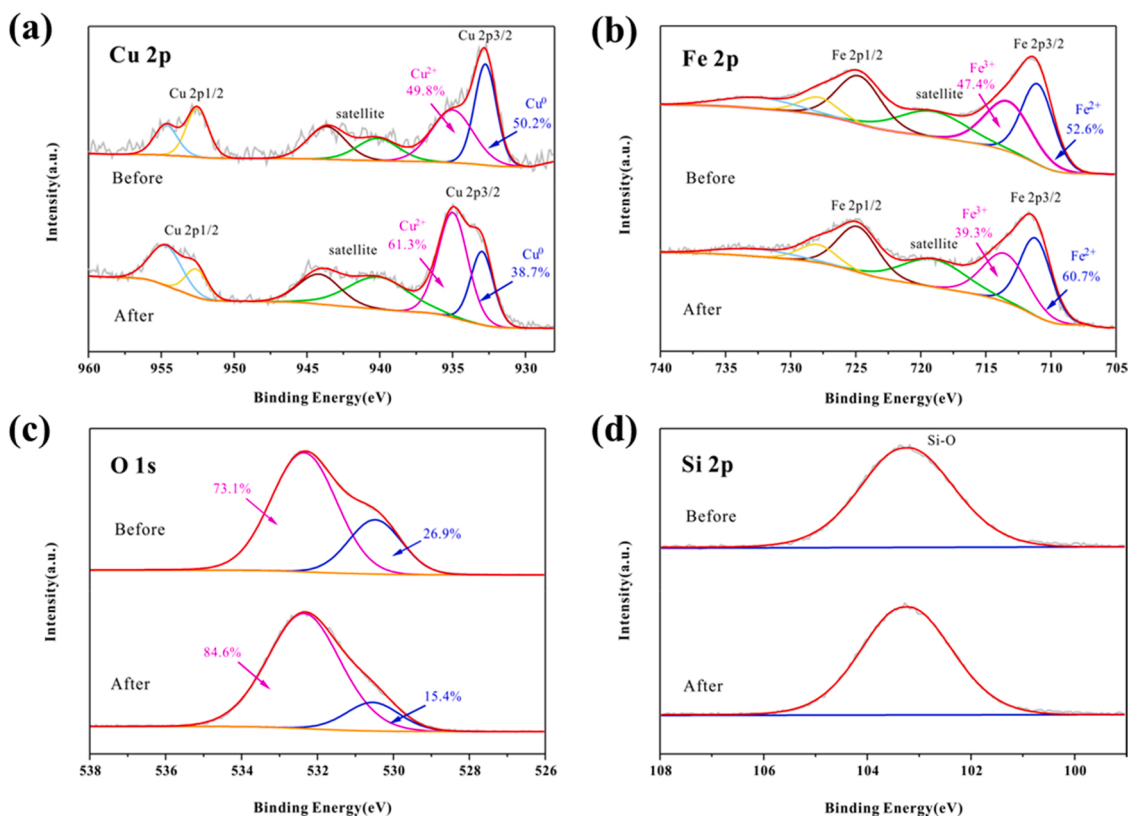


Fig. 5. XPS spectra of Cu 2p (a), Fe 2p (b), O 1s (c), Si 2p (d) for Cu/CuFe₂O₄/DE composite.

variations were obtained by deconvolving Cu2p, O1s, Fe2p, and Si2p spectral signatures. The Cu2p signal deconvolved into six peaks; the satellite peaks at 932.74 eV and 952.52 eV correspond to Cu⁰ and the peaks at 940.13 eV, 943.65 eV, 935.01 eV, and 954.69 eV correspond to the presence of Cu²⁺ [48–50]. When TC degraded by Cu/CuFe₂O₄/DE via a Fenton-like process, the % mole Cu⁰ of the used catalyst decreased from 50.2 % to 38.7 % showing Cu⁰ → Cu²⁺ conversion.

Similarly, in Cu/CuFe₂O₄/DE (both pristine and spent) the iron occurs in Fe²⁺, and Fe³⁺ valence states as shown by the Fe2p deconvoluted peaks at 711.02 eV and 724.74 eV, and 719.10 eV, respectively [51,52]. As the Cu/CuFe₂O₄/DE assisted Fenton-like process commences for TC degradation, the %mole of Fe²⁺ has increased from 52.6 % to 60.7 % showing Fe³⁺ → Fe²⁺ reduction. The surface Fe³⁺ may also consume via Cu⁰ oxidation. However, the XPS spectral data shown here is not adequate to isolate these two processes. The O1s spectrum of the Cu/CuFe₂O₄/DE composite shows two peaks corresponding to lattice-bound O (530.48 eV) and surface hydroxyls (532.36 eV) which act as a nucleus in generating hydroxyl radicals required for a Fenton-like process [53]. The % mole composition of lattice O has decreased from 26.9 % to 15.4 % and the percentage of OH component of indicating that hydroxylation occurred on the surface during the catalytic reaction [54]. The peak at 103 eV of the Si 2p corresponds to the Si-O bond which shows negligible variation in both composites [32] which implies the role of DE as catalyst support.

3.2. Fenton-like catalytic activity of Cu/CuFe₂O₄/DE composites

The Fenton-like performance of the Cu/CuFe₂O₄/DE was examined against Cu/DE, CuFe₂O₄/DE, CuFe₂O₄, and Cu/CuFe₂O₄ measuring TC degradation efficiency. As shown in Fig. 6(a), when H₂O₂ is added in the absence of a catalyst, the TC content in the reaction system does not change significantly with the contact time, indicating that H₂O₂ oxidation has negligible TC degradation. In the presence of the catalyst, the TC degradation efficiency approximates 100 % within 90 min, showing

that Cu/CuFe₂O₄/DE has a marked activation effect on H₂O₂.

The Fenton-like effect of the substrates, e.g., CuFe₂O₄, CuFe₂O₄/DE, Cu/CuFe₂O₄, Cu/DE, Cu/CuFe₂O₄, and Cu/CuFe₂O₄/DE and H₂O₂ on the TC degradation was also examined (Fig. 6.b). Before evaluating the catalytic properties of the catalysts, the TC adsorption experiments were performed in the dark (shown in Fig. S2). The adsorption equilibria of the catalysts were reached in about 30 min. The efficiency of TC degradation depends on the type of catalyst used. When CuFe₂O₄/H₂O₂ was used less than 30 % TC degraded or removed from the solution. The CuFe₂O₄ coagulate readily thus reducing its electron shuttling efficiency. When Cu/DE/H₂O₂ is used, the degree of TC degradation is increased to about 50 % due to the activation of Cu⁰/Cu⁺/Cu²⁺ redox sites for electron exchange (Fig. 6.b). Interestingly, when Cu/CuFe₂O₄/H₂O₂ is used, the TC degradation rate is enhanced significantly. The Cu⁺/Cu²⁺ and Fe²⁺/Fe³⁺ redox states on Cu/CuFe₂O₄ promote electron transfer with H₂O₂ for the production of hydroxyl radicals, resulting in over 85 % TC degradation. However, the coagulation of Cu/CuFe₂O₄ particulates hinders the efficiency of the Fenton-like process. In contrast, when the Cu/CuFe₂O₄ are dispersed on DE, particulates agglomeration is reduced significantly as exemplified by enhanced TC degradation rate, viz. over 95 % with Cu/CuFe₂O₄/DE and H₂O₂.

As shown in Fig. S3, the catalytic performance of the Cu/CuFe₂O₄/DE was enhanced with the amount of diatomite used. At a given mass of the catalyst when diatomite content is increased beyond 0.7 g, the catalyst activity is somewhat reduced due to the dilution of the active sites.

The effect of H₂O₂ concentration on the degradation of TC was also investigated (Fig. 6.c). The rate of TC degradation by Cu/CuFe₂O₄/DE increases exponentially with the [H₂O₂] at a given catalyst concentration reaching an optimal when [H₂O₂] > 4 mM. This points to the saturation of surface sites with the H₂O₂. The solution pH also exerts a marked effect showing the highest TC degradation by Cu/CuFe₂O₄/DE at acidic conditions (pH < 3). When solution pH increases the TC degradation efficiency shows a marked reduction due to the rapid

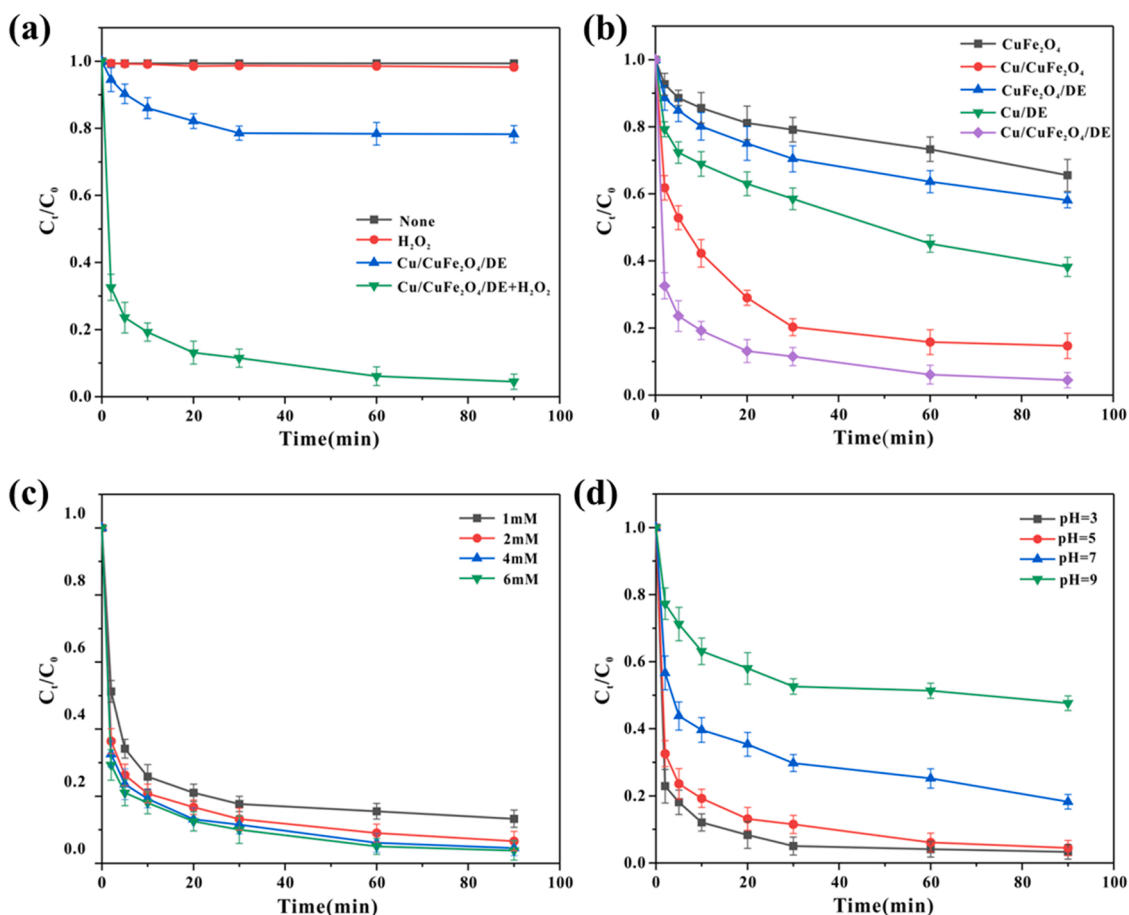


Fig. 6. (a) Effect of different reaction systems on the degradation rate of TC; (b) Effect of different catalysts on the degradation rate of TC; (c) Effect of different H_2O_2 dosages on the degradation rate of TC; (d) Effect of initial pH on TC degradation in the Cu/CuFe₂O₄/DE/ H_2O_2 system. (Reaction conditions: pH 5.0; initial TC, 50 mg/L; catalyst, 200 mg/L; H_2O_2 , 4.0 mM).

conversion of Fe^{2+} and Fe^{3+} into iron oxyhydroxides, thus passivating the catalyst (Fig. 6.d) [55,56]. As pH increases the H_2O_2 undergoes spontaneous decomposition which further inhibits the free radical production required for TC degradation [57]. Furthermore, the adsorption of TC by Cu/CuFe₂O₄ under different pH conditions was also investigated. The zeta potential of Cu/CuFe₂O₄/DE was measured by a zeta potentiometer. As shown in Fig S4, the pHzpc of Cu/CuFe₂O₄/DE is 7.12. When the pH of the solution is lower than 7.12, the

Cu/CuFe₂O₄/DE is positively charged and when the pH is greater than 7.12, the Cu/CuFe₂O₄/DE is negatively charged. In the pH range of 3.3–7.7, TC behaves as a zwitterionic form, and in the range of pH below 3.3, TC is cationic species [58]. When the pH of the reaction system is 3, the positively charged Cu/CuFe₂O₄/DE and the cationic form of TC repel each other due to electrostatic interaction, and the adsorption of TC by Cu/CuFe₂O₄/DE decreases but still maintains excellent TC removal rates. Therefore, the removal of TC in the Cu/CuFe₂O₄/DE + H_2O_2

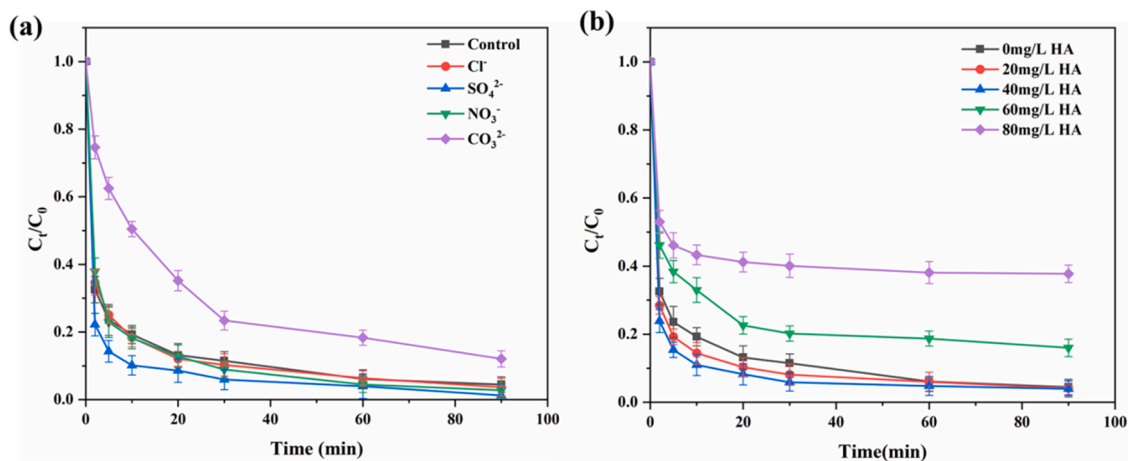


Fig. 7. (a) The effect of common anions on TC degradation in Cu/CuFe₂O₄/DE system; (b) The effect of HA on TC degradation in Cu/CuFe₂O₄/DE system. (Reaction conditions: pH 5.0; initial TC, 50 mg/L; catalyst, 200 mg/L; H_2O_2 , 4.0 mM).

reaction system is mainly attributed to the catalytic degradation process.

Natural water and wastewater contain a variety of ions and other solutes that exert an impact on the performance of Fenton-like catalysts [59]. The effect of Cl^- , SO_4^{2-} , NO_3^- , CO_3^{2-} and natural organic matter on the degradation of TC by Cu/CuFe₂O₄/DE/H₂O₂ was examined. As shown in Fig. 7(a), in the presence of CO_3^{2-} , the degradation efficiency of TC decreased significantly due to its competing effect with TC for $\bullet\text{OH}$ capturing [60]. On the other hand, SO_4^{2-} reacts with $\bullet\text{OH}$ forming reactive new free radicals [61], therefore the presence of SO_4^{2-} promotes the efficiency of Cu/CuFe₂O₄/DE. However, the presence of Cl^- or NO_3^- in solution exerts a negligible role in TC degradation. Therefore, the activity of Cu/CuFe₂O₄/DE sustains at a steady state despite the contrasting behavior of various solute species present in free radicals' production.

Humic acid fractions (HA), e.g., 30–50 % of total organic matter are ubiquitous in water [62]. As shown in Fig. S5, when $[\text{HA}] < 40 \text{ mg/L}$, the TC degradation rate increases slightly with the $[\text{HA}]$ thus promoting $\text{Fe}^{3+} \rightarrow \text{Fe}^{2+}$ conversion [63]. HA usually has a high density of oxygen-containing functional groups and can be used in electron shuttling and metal ions complexing, improving the electron transfer efficiency and oxidation process [64]. HA recombines with iron ions to form complexes that reduce the redox potential between $\text{Fe}^{3+}/\text{Fe}^{2+}$ cycles, thus promoting the conversion of $\text{Fe}^{3+} \rightarrow \text{Fe}^{2+}$ [65]. When the $[\text{HA}] > 40 \text{ mg/L}$, the TC degradation efficiency decreases significantly with the $[\text{HA}]$, as it can absorb Cu/CuFe₂O₄/DE by poisoning the catalyst. Further, HA and TC compete for $\bullet\text{OH}$ resulting apparent reduction of the TC degradation efficiency.

The effect of the initial $[\text{TC}]$ concentration as a function of its degradation by Cu/CuFe₂O₄/DE/H₂O₂ was examined as shown in Fig. S5. As the $[\text{TC}]$ increases its degradation efficiency is reduced significantly due to the limited availability of active sites on Cu/CuFe₂O₄/DE and the scavenging of free radicals by intermediate products (Fig. S5). During the experiment, we also conducted degradation tests on other kinds of antibiotic pollutants (sulfamethoxazole, oxytetracycline), and found that Cu/CuFe₂O₄/DE also had excellent catalytic degradation performance, the experimental results are shown in Fig S6.

3.3. Possible degradation pathways of TC

The intermediates of TC degradation by Cu/CuFe₂O₄/DE/H₂O₂ system were determined by high-performance liquid chromatography-mass spectrometry (HPLC-MS) and 11 intermediates are identified as given in Table S1. Accordingly, as shown in Fig. 8, two routes for TC degradation by Cu/CuFe₂O₄/DE/H₂O₂ can be suggested.

In the Fenton-like process, the electron-rich double bonds, phenolic and amide groups in TC are easily attacked by the electrophilic $\bullet\text{OH}$ radicals [66]. For pathway I, the C=C bond reacts with $\bullet\text{OH}$ radical first, and then the double bond is opened to form hydroxyl and carbonyl groups, respectively, yielding P1 ($m/z = 461$) and P2 ($m/z = 477$) intermediates [67]. The dimethylamine group on P2 is further attacked by $\bullet\text{OH}$, deamidated, while the ortho and para positions of the phenol ring are also attacked by $\bullet\text{OH}$, forming ketones and P3 ($m/z = 362$)

intermediates [68]. Then, P4 ($m/z = 280$) was further dehydrated and oxidized by $\bullet\text{OH}$. Under the action of $\bullet\text{OH}$ and $\bullet\text{O}_2^-$, P4 was degraded through ring opening and loss of functional groups to produce smaller organic molecules, P5 ($m/z = 149$) and P6 ($m/z = 145$) [69]. In pathway II, the benzene ring is first opened to generate P7 ($m/z = 509$) intermediate, the C=C bond is opened, P7 is degraded to P8 ($m/z = 525$), and P8 deamidation, dehydration, and hydroxyl group form P9 ($m/z = 367$) [70]. Subsequently, smaller organic molecules P10 ($m/z = 146$) and P11 ($m/z = 116$) are formed by ring opening and demethylation. Eventually, the smaller organic molecular intermediates P5, P6, P10, and P11 are mineralized into H₂O and CO₂ [71].

3.4. Fenton-like degradation mechanism of TC

To further investigate the mechanism of Fenton-like catalytic reactions, the active free radicals produced in the Cu/CuFe₂O₄/DE/H₂O₂ system were explored by quenching experiments. In the Fenton-like process, hydroxyl radicals ($\bullet\text{OH}$) and superoxide radicals ($\bullet\text{O}_2^-$) are generally considered to be the active species. Tert-butanol (TBA) and p-benzoquinone (BQ) were selected as quenchers of $\bullet\text{OH}$ and $\bullet\text{O}_2^-$, respectively [72]. As shown in Fig. 9, with the addition of BQ, the degradation effect of TC was slightly inhibited, indicating that $\bullet\text{O}_2^-$ may not be important in TC degradation. In contrast, the degradation of TC was significantly inhibited after adding TBA, which indicated that $\bullet\text{OH}$ played a major role in the degradation of TC.

The production of $\bullet\text{OH}$ and $\bullet\text{O}_2^-$ radicals by aqueous H₂O₂ in the presence or absence of Cu/CuFe₂O₄/DE was examined by electron spin spectroscopy (ESR) using DMPO free radical capturing agent. When only an aqueous H₂O₂ solution was used no ESR signals corresponding to $\bullet\text{OH}$ or $\bullet\text{O}_2^-$ can be detected. However, when Cu/CuFe₂O₄/DE is introduced into the H₂O₂ solution, the ESR signals corresponding to both $\bullet\text{OH}$ and $\bullet\text{O}_2^-$ can be detected (Fig. 10. a and b). Accordingly, a postulated TC degradation by H₂O₂ in the presence of Cu/CuFe₂O₄/DE is presented.

According to the experimental results so far presented, the possible reaction mechanism of TC degradation by Cu/CuFe₂O₄/DE/H₂O₂ is proposed as shown in Fig. 11. Under acidic conditions, Fe^{3+} and Cu^{2+} present in Cu/CuFe₂O₄/DE react with H₂O₂ to form Fe^{2+} and Cu^+ (Eqs. (1) and (2)) [73]. The Fe^{2+} and Cu^+ then further react with H₂O₂ to generate $\bullet\text{OH}$ by $\text{Fe}^{2+} \rightarrow \text{Fe}^{3+}$ and $\text{Cu}^+ \rightarrow \text{Cu}^{2+}$ conversion in a cyclic fashion (Eqs. (3) and (4)) [74]. At the same time, some portion of Fe^{3+} reacts with $\bullet\text{O}_2\text{H}$ to form $\bullet\text{O}_2^-$ (Eq. (5)). In addition, Cu^0 and Cu^+ in Cu/CuFe₂O₄/DE can donate electrons to reduce $\text{Fe}^{3+} \rightarrow \text{Fe}^{2+}$, by Cu^0 and Cu^+ via a rapid conversion cycle (Eqs. (6) and (7)) [54,75]. According to the XPS data, the role of Cu^0 in reducing Fe^{3+} to Fe^{2+} is shown in postulating the proposed mechanism (Fig. 11). In summary, the synergy between $\text{Cu}^0/\text{Cu}^{2+}$ and $\text{Fe}^{2+}/\text{Fe}^{3+}$ cyclic conversion improves the catalytic performance of Cu/CuFe₂O₄/DE/H₂O₂.

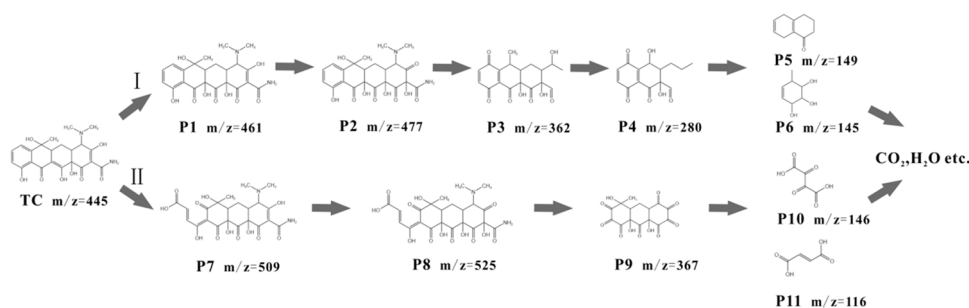


Fig. 8. Proposed degradation pathways of TC in the Cu/CuFe₂O₄/DE Fenton-like system.

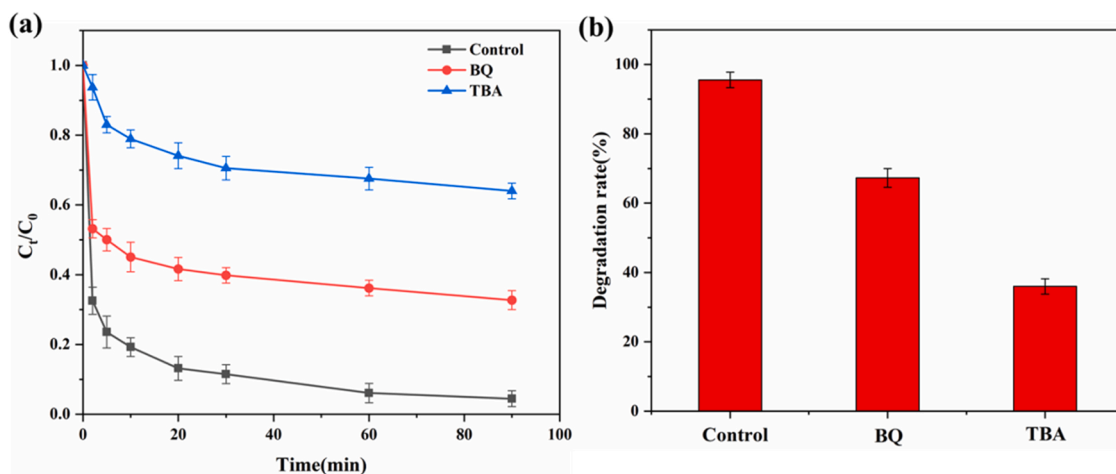


Fig. 9. (a) and (b) Effect of radical scavengers on the degradation of TC (Reaction conditions: pH 5.0; initial TC, 50 mg/L; catalyst, 200 mg/L; H_2O_2 , 4.0 mM).

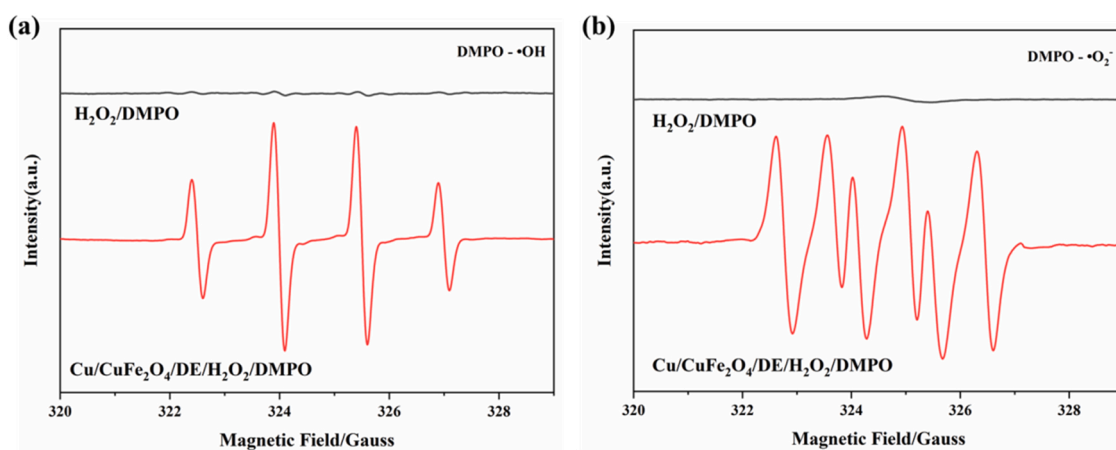


Fig. 10. ESR spectra of $\bullet OH$ (a) and $\bullet O_2^-$ (b) generated by $Cu/CuFe_2O_4/DE$.

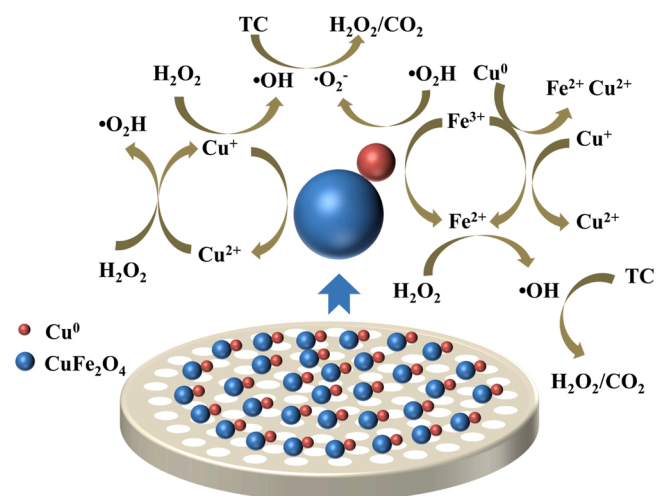
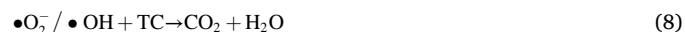


Fig. 11. The Schematic diagram of TC degradation by $Cu/CuFe_2O_4/DE$ composites in Fenton-like systems.



3.5. Catalyst stability and reusability

The stability and reusability of the $Cu/CuFe_2O_4/DE$ composite were determined by measuring its metal ion leaching propensity and the catalyst activity deterioration upon repeated use for TC degradation. As shown in Fig. 12(a), with the introduction of diatomite, the Cu^{2+} and Fe^{2+} leaching from $Cu/CuFe_2O_4/DE$ reduced significantly due to their surface complexing with $\equiv SiOH$ sites on porous diatomite. In addition, the recyclability of the used catalyst on TC degradation was also investigated. Spinel-type $CuFe_2O_4$ has strong magnetic properties. Fig. S6 shows the hysteresis loop of the $Cu/CuFe_2O_4$ nanocomposite with an applied magnetic field of ± 2 T. After $Cu/CuFe_2O_4$ loading onto diatomite, the intensity of saturation magnetization (M_s) of $Cu/CuFe_2O_4/DE$ decreases slightly; however, the reduced magnetic

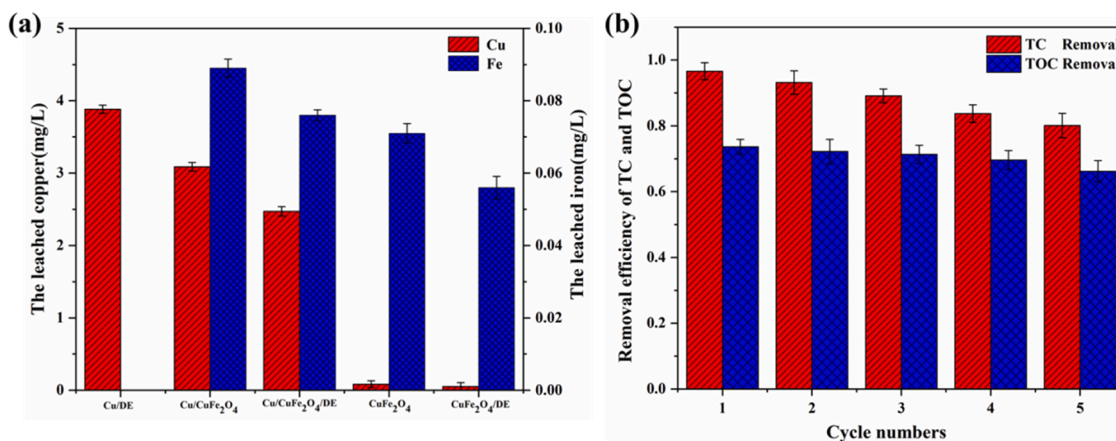


Fig. 12. (a) Leaching amount of copper and iron ions from catalyst;(b) Removal efficiency of TOC and TC. (Reaction conditions: pH 5.0; initial TC, 50 mg/L; catalyst, 200 mg/L; H₂O₂, 4.0 mM).

intensity is still adequate to separate spent particulates from the reaction mixture (Fig. S7). To explore the reusability of the spent Cu/CuFe₂O₄/DE catalyst, the TC degradation experiments were also carried out under an identical experimental setup for five cycles. As shown in Fig. 12(b), after five cycles, the TC removal rate by spent Cu/CuFe₂O₄/DE is maintained at 80 %, and the TOC mineralization rate of TC is maintained at 66 %, showing its sustained reactivity. In conclusion, the results show that the Cu/CuFe₂O₄/DE composite has good stability and repeatability.

4. Conclusion

Presently, Cu/CuFe₂O₄/DE composites, prepared by a one-step solvothermal method, were used as a heterogeneous Fenton-like catalyst to degrade TC under acidic conditions. The excellent catalytic performance of Cu/CuFe₂O₄/DE is due to its large specific surface area, better pore size distribution, and abundant surface-active sites. The degradation rate of Cu/CuFe₂O₄/DE remains above 80 % after 5 consecutive cycles, showing high stability and reusability. The diatomite carrier can not only solve the Cu/CuFe₂O₄ agglomeration problem but also limit the leaching of metal ions in the catalyst, which is due to its complexation with the silica hydroxyl group and the pore limitation effect of diatomite. The introduction of Cu⁰ enhances the catalytic activity of the material, and the synergy between Cu⁺/Cu²⁺ and Fe²⁺/Fe³⁺ redox pairs enhanced the generation of free radicals required for TC degradation. Hydroxyl radical played a leading role in the degradation and removal of TC during the reaction. The work of this paper provides a new idea for the preparation of heterogeneous Fenton-like catalysts with high catalytic efficiency and good reuse by combining diatomite, Cu⁰, and CuFe₂O₄.

CRediT authorship contribution statement

Shuai Deng: Methodology, Validation, Writing – original draft, Funding acquisition; **Zhi Guo:** Methodology, Writing – review & editing; **Yi-Han Chen:** Methodology, Validation; **Kang-Ping Cui:** Methodology, Validation; **Zhao-Gang Ding:** Methodology, Writing – review & editing; **Bei Wang:** Methodology; **Rohan Weerasooriya:** Writing – review & editing; **Xing Chen:** Validation, Investigation, Writing – review & editing.

Declaration of Competing Interest

The authors declare that they have no known competing financial interests or personal relationships that could have appeared to influence the work reported in this paper.

Data availability

Data will be made available on request.

Acknowledgments

The authors acknowledge the financial support from the Key Science and Technology Projects of Anhui Province (202003a07020004), and the National Key R&D Program of China (2019YFC0408500). R. W. acknowledges the Program of Distinguished Professor in B&R Countries (Grant No. G20200012010).

Appendix A. Supporting information

Supplementary data associated with this article can be found in the online version at [doi:10.1016/j.jece.2023.110045](https://doi.org/10.1016/j.jece.2023.110045).

References

- [1] Y.Y. Liu, Y. Wang, T.R. Walsh, L.X. Yi, R. Zhang, J. Spencer, Y. Doi, G.B. Tian, B. L. Dong, X.H. Huang, L.F. Yu, D.X. Gu, H.W. Ren, X.J. Chen, L.C. Lv, D.D. He, H. W. Zhou, Z.S. Liang, J.H. Liu, J.Z. Shen, Emergence of plasmid-mediated colistin resistance mechanism MCR-1 in animals and human beings in China: a microbiological and molecular biological study, *Lancet Infect. Dis.* 16 (2) (2016) 161–168.
- [2] R. Daghrir, P. Drogui, Tetracycline antibiotics in the environment: a review, *Environ. Chem. Lett.* 11 (3) (2013) 209–227.
- [3] W. Dai, L. Jiang, J. Wang, Y. Pu, Y. Zhu, Y. Wang, B. Xiao, Efficient and stable photocatalytic degradation of tetracycline wastewater by 3D Polyaniline/Perylene diimide organic heterojunction under visible light irradiation, *Chem. Eng. J.* (2020) 397.
- [4] N.A. Al-Dhabi, G.A. Esmail, M.V. Arasu, Effective degradation of tetracycline by manganese peroxidase producing *Bacillus velezensis* strain Al-Dhabi 140 from Saudi Arabia using fibrous-bed reactor, *Chemosphere* (2021) 268.
- [5] Y.K. Shi, H. Lin, J.W. Ma, R.R. Zhu, W.C. Sun, X.Y. Lin, J. Zhang, H.B. Zheng, X. Zhang, Degradation of tetracycline antibiotics by *Arthrobacter nicotianae* OTC-16, *J. Hazard Mater.* (2021) 403.
- [6] D. Jiang, T. Wang, Q. Xu, D. Li, S. Meng, M. Chen, Perovskite oxide ultrathin nanosheets/g-C₃N₄ 2D–2D heterojunction photocatalysts with significantly enhanced photocatalytic activity towards the photodegradation of tetracycline, *Appl. Catal. B-Environ.* 201 (2017) 617–628.
- [7] S.C. Kim, K. Carlson, Temporal and spatial trends in the occurrence of human and veterinary antibiotics in aqueous and river sediment matrices, *Environ. Sci. Technol.* 41 (1) (2007) 50–57.
- [8] K. Kuehmerer, Antibiotics in the aquatic environment - a review - Part I, *Chemosphere* 75 (4) (2009) 417–434.
- [9] M. Ahmadi, H.R. Motlagh, N. Jaafarzadeh, A. Mostoufi, R. Saeedi, G. Barzegar, S. Jorfi, Enhanced photocatalytic degradation of tetracycline and real pharmaceutical wastewater using MWCNT/TiO₂ nano-composite, *J. Environ. Manag.* 186 (2017) 55–63.
- [10] J. Hou, C. Wang, D. Mao, Y. Luo, The occurrence and fate of tetracyclines in two pharmaceutical wastewater treatment plants of Northern China, *Environ. Sci. Pollut. Res.* 23 (2) (2016) 1722–1731.

- [11] J. Cui, X.R. Xu, L.Y. Yang, C.T. Chen, J.S. Qian, X. Chen, D.P. Sun, Soft foam-like UiO-66/Polydopamine/Bacterial cellulose composite for the removal of aspirin and tetracycline hydrochloride, *Chem. Eng. J.* (2020) 395.
- [12] H.S. Chen, M.H. Huang, Z.W. Wang, P. Gao, T. Cai, J.L. Song, Y.Y. Zhang, L. J. Meng, Enhancing rejection performance of tetracycline resistance genes by a TiO₂/AgNPs-modified nanofiber forward osmosis membrane, *Chem. Eng. J.* (2020) 382.
- [13] Z. Lin, Z. Zhen, S. Luo, L. Ren, Y. Chen, W. Wu, W. Zhang, Y.-Q. Liang, Z. Song, Y. Li, D. Zhang, Effects of two ecological earthworm species on tetracycline degradation performance, pathway and bacterial community structure in laterite soil, *J. Hazard Mater.* (2021) 412.
- [14] X.D. Zhu, Y.J. Wang, R.J. Sun, D.M. Zhou, Photocatalytic degradation of tetracycline in aqueous solution by nanosized TiO₂, *Chemosphere* 92 (8) (2013) 925–932.
- [15] J. Jeong, W.H. Song, W.J. Cooper, J. Jung, J. Greaves, Degradation of tetracycline antibiotics: Mechanisms and kinetic studies for advanced oxidation/reduction processes, *Chemosphere* 78 (5) (2010) 533–540.
- [16] X.H. Wen, Y.N. Jia, J.X. Li, Enzymatic degradation of tetracycline and oxytetracycline by crude manganese peroxidase prepared from *Phanerochaete chrysosporium*, *J. Hazard Mater.* 177 (1–3) (2010) 924–928.
- [17] X. Chen, Y. Ke, Y. Zhu, M. Xu, C. Chen, S. Xie, Enrichment of tetracycline-degrading bacterial consortia: Microbial community succession and degradation characteristics and mechanism, *J. Hazard Mater.* 448 (2023), 130984 (-).
- [18] F. Shi, H. Shan, D. Li, X. Yin, J. Yu, B. Ding, A general strategy to fabricate soft magnetic CuFe₂O₄@SiO₂ nanofibrous membranes as efficient and recyclable Fenton-like catalysts, *J. Colloid Interface Sci.* 538 (2019) 620–629.
- [19] C. Liu, Y.P. Wang, Y.T. Zhang, R.Y. Li, W.D. Meng, Z.L. Song, F. Qi, B.B. Xu, W. Chu, D.H. Yuan, B. Yu, Enhancement of Fe@porous carbon to be an efficient mediator for peroxymonosulfate activation for oxidation of organic contaminants: Incorporation NH₂-group into structure of its MOF precursor, *Chem. Eng. J.* 354 (2018) 835–848.
- [20] Z. Liu, K. Demeestere, S. Van Hulle, Pretreatment of secondary effluents in view of optimal ozone-based AOP removal of trace organic contaminants: bench-scale comparison of efficiency and energy consumption, *Ind. Eng. Chem. Res.* 59 (16) (2020) 8112–8120.
- [21] L.W. Chen, D.H. Ding, C. Liu, H. Cai, Y. Qu, S.J. Yang, Y. Gao, T.M. Cai, Degradation of norfloxacin by CoFe₂O₄-GO composite coupled with peroxymonosulfate: a comparative study and mechanistic consideration, *Chem. Eng. J.* 334 (2018) 273–284.
- [22] H. Katsumata, S. Kaneco, T. Suzuki, K. Ohta, Y. Yobiko, Degradation of linuron in aqueous solution by the photo-Fenton reaction, *Chem. Eng. J.* 108 (3) (2005) 269–276.
- [23] Z. Cui, P. Wang, X. Liu, X. Liang, Q. Zhang, Z. Wang, Z. Zheng, H. Cheng, Y. Liu, Y. Dai, B. Huang, Design and synthesis of BiVO₄@CuO_x as a photo assisted Fenton-like catalyst for efficient degradation of tetracycline, *Surf. Interfaces* (2021) 26.
- [24] M. Cheng, G.M. Zeng, D.L. Huang, C. Lai, P. Xu, C. Zhang, Y. Liu, J. Wan, X. M. Gong, Y. Zhu, Degradation of atrazine by a novel Fenton-like process and assessment the influence on the treated soil, *J. Hazard Mater.* 312 (2016) 184–191.
- [25] Y. Yao, F. Lu, Y. Zhu, F. Wei, X. Liu, C. Lian, S. Wang, Magnetic core-shell CuFe₂O₄@C₃N₄ hybrids for visible light photocatalysis of Orange II, *J. Hazard Mater.* 297 (2015) 224–233.
- [26] C.R. Keenan, D.L. Sedlak, Ligand-enhanced reactive oxidant generation by nanoparticulate zero-valent iron and oxygen, *Environ. Sci. Technol.* 42 (18) (2008) 6936–6941.
- [27] J. Khatri, P.V. Nidheesh, S.A. Singh, M.S. Kumar, Advanced oxidation processes based on zero-valent aluminium for treating textile wastewater, *Chem. Eng. J.* 348 (2018) 67–73.
- [28] P. Zhou, J. Zhang, Y.L. Zhang, G.C. Zhang, W.S. Li, C.M. Wei, J. Liang, Y. Liu, S. H. Shu, Degradation of 2,4-dichlorophenol by activating persulfate and peroxymonosulfate using micron or nanoscale zero-valent copper, *J. Hazard Mater.* 344 (2018) 1209–1219.
- [29] H.H. Zhang, B.P. Cao, W.P. Liu, K.D. Lin, J. Feng, Oxidative removal of acetaminophen using zero valent aluminium-acid system: Efficacy, influencing factors, and reaction mechanism, *J. Environ. Sci. -China* 24 (2) (2012) 314–319.
- [30] P. Zhou, J. Zhang, Y.L. Zhang, J. Liang, Y. Liu, B. Liu, W. Zhang, Activation of hydrogen peroxide during the corrosion of nanoscale zero valent copper in acidic solution, *J. Mol. Catal. a-Chem.* 424 (2016) 115–120.
- [31] Y. Ding, Y. Ruan, L. Zhu, H. Tang, Efficient oxidative degradation of chlorophenols by using magnetic surface carboxylated Cu(0)/Fe₃O₄ nanocomposites in a wide pH range, *J. Environ. Chem. Eng.* 5 (3) (2017) 2681–2690.
- [32] Y. Tan, C. Li, Z. Sun, R. Bian, X. Dong, X. Zhang, S. Zheng, Natural diatomite mediated spherically monodispersed CoFe₂O₄ nanoparticles for efficient catalytic oxidation of bisphenol A through activating peroxymonosulfate, *Chem. Eng. J.* (2020) 388.
- [33] A. Alpay, O. Tuna, E.B. Simsek, Deposition of perovskite-type LaFeO₃ particles on spherical commercial polystyrene resin: a new platform for enhanced photo-Fenton-catalyzed degradation and simultaneous wastewater purification, *Environ. Technol. Innov.* (2020) 20.
- [34] B. Janani, M.K. Okla, M.A. Abdel-Maksoud, H. Abdelgawad, A.M. Thomas, L. L. Raju, W.H. Al-Qahtani, S.S. Khan, CuO loaded ZnS nanoflower entrapped on PVA-chitosan matrix for boosted visible light photocatalysis for tetracycline degradation and anti-bacterial application, *J. Environ. Manag.* (2022) 306.
- [35] O. Tuna, E.B. Simsek, Anchoring LaFeO₃ perovskites on the polyester filters for flowthrough photocatalytic degradation of organic pollutants, *J. Photochem. Photobiol. A* (2021) 418.
- [36] C. Xiong, Q. Ren, X. Liu, Z. Jin, Y. Ding, H. Zhu, J. Li, R. Chen, Fenton activity on RhB degradation of magnetic g-C₃N₄/diatomite/Fe₃O₄ composites, *Appl. Surf. Sci.* (2021) 543.
- [37] P. Zhu, Y. Chen, M. Duan, M. Liu, P. Zou, Structure and properties of Ag₃PO₄/diatomite photocatalysts for the degradation of organic dyes under visible light irradiation, *Powder Technol.* 336 (2018) 230–239.
- [38] S.Y. Wang, W.J. An, J.R. Lu, L. Liu, J.S. Hu, Y.H. Liang, W.Q. Cui, A Cu/CuFe₂O₄-OVs two-electron centre-based synergistic photocatalysis-Fenton system for efficient degradation of organic pollutants, *Chem. Eng. J.* (2022) 441.
- [39] Z.P. Liu, Y. Yang, J.B. Liang, Z.K. Hu, S. Li, S. Peng, Y.T. Qian, Synthesis of copper nanowires via a complex-surfactant-assisted hydrothermal reduction process, *J. Phys. Chem. B* 107 (46) (2003) 12658–12661.
- [40] J. Feng, L. Su, Y. Ma, C. Ren, Q. Guo, X. Chen, CuFe₂O₄ magnetic nanoparticles: a simple and efficient catalyst for the reduction of nitrophenol, *Chem. Eng. J.* 221 (2013) 16–24.
- [41] X. Dong, B. Ren, Z. Sun, C. Li, X. Zhang, M. Kong, S. Zheng, D.D. Dionysiou, Monodispersed CuFe₂O₄ nanoparticles anchored on natural kaolinite as highly efficient peroxymonosulfate catalyst for bisphenol A degradation, *Appl. Catal. B-Environ.* 253 (2019) 206–217.
- [42] Y. Zhang, X. Chen, M.-S. Cui, Z. Guo, Y.-H. Chen, K.-P. Cui, Z.-G. Ding, R. Weerasooriya, Binding Fe-doped g-C₃N₄ on the porous diatomite for efficient degradation of tetracycline via photo-Fenton process, *J. Environ. Chem. Eng.* 10 (3) (2022).
- [43] S.M. Fotukian, A. Barati, M. Soleymani, M. Alizadeh, Solvothermal synthesis of CuFe₂O₄ and Fe₃O₄ nanoparticles with high heating efficiency for magnetic hyperthermia application, *J. Alloy. Compd.* 816 (2020).
- [44] S. Wu, C.Z. Wang, Y.Q. Jin, G.Z. Zhou, L.Y. Zhang, P.P. Yu, L.G. Sun, Green synthesis of reusable super-paramagnetic diatomite for aqueous nickel (II) removal, *J. Colloid Interface Sci.* 582 (2021) 1179–1190.
- [45] P.V. Viet, D.V. Chuyen, N.Q. Hien, N.N. Duy, C.M. Thi, Visible-light-induced photo-Fenton degradation of rhodamine B over Fe₂O₃-diatomite materials, *J. Sci. -Adv. Mater. Dev.* 5 (3) (2020) 308–315.
- [46] B. Krishnakumar, T. Imae, J. Miras, J. Esquena, Synthesis and azo dye photodegradation activity of ZrS₂-ZnO nano-composites, *Sep. Purif. Technol.* 132 (2014) 281–288.
- [47] X. Zhang, Y. Ding, H. Tang, X. Han, L. Zhu, N. Wang, Degradation of bisphenol A by hydrogen peroxide activated with CuFe₂O₄ microparticles as a heterogeneous Fenton-like catalyst: efficiency, stability and mechanism, *Chem. Eng. J.* 236 (2014) 251–262.
- [48] Z. Li, J. Lyu, M. Ge, Synthesis of magnetic Cu/CuFe₂O₄ nanocomposite as a highly efficient Fenton-like catalyst for methylene blue degradation, *J. Mater. Sci.* 53 (21) (2018) 15081–15095.
- [49] Y.T. Zhang, C. Liu, B.B. Xu, F. Qi, W. Chu, Degradation of benzotriazole by a novel Fenton-like reaction with mesoporous Cu/MnO_x: combination of adsorption and catalysis oxidation, *Appl. Catal. B-Environ.* 199 (2016) 447–457.
- [50] Y.C. Dong, Y.S. Chui, R.G. Ma, C.W. Cao, H. Cheng, Y.Y. Li, J.A. Zapien, One-pot scalable synthesis of Cu-CuFe₂O₄/graphene composites as anode materials for lithium-ion batteries with enhanced lithium storage properties, *J. Mater. Chem. A* 2 (34) (2014) 13892–13897.
- [51] Y.P. Bao, T.T. Lim, R. Wang, R.D. Webster, X. Hu, Urea-assisted one-step synthesis of cobalt ferrite impregnated ceramic membrane for sulfamethoxazole degradation via peroxymonosulfate activation, *Chem. Eng. J.* 343 (2018) 737–747.
- [52] L. Lu, Z. Ai, J. Li, Z. Zheng, Q. Li, L. Zhang, Synthesis and characterization of Fe-Fe₂O₃ core-shell nanowires and nanonecklaces, *Cryst. Growth Des.* 7 (2) (2007) 459–464.
- [53] S. Xing, Z. Zhou, Z. Ma, Y. Wu, Characterization and reactivity of Fe₃O₄/FeMnO_x core/shell nanoparticles for methylene blue discoloration with H₂O₂, *Appl. Catal. B-Environ.* 107 (3–4) (2011) 386–392.
- [54] X. Wu, F. Xia, Z. Nan, Facile synthesis of double-mesoporous-shelled hollow spheres of Cu-CuFe₂O₄/SiO₂ composite as excellent Fenton catalyst, *Mater. Chem. Phys.* (2020) 242.
- [55] X. Liu, Z. Cao, Z.L. Yuan, J. Zhang, X.P. Guo, Y. Yang, F. He, Y.P. Zhao, J. Xu, Insight into the kinetics and mechanism of removal of aqueous chlorinated nitroaromatic antibiotic chloramphenicol by nanoscale zero-valent iron, *Chem. Eng. J.* 334 (2018) 508–518.
- [56] J.F. Bai, Y. Liu, X.H. Yin, H.T. Duan, J.H. Ma, Efficient removal of nitrobenzene by Fenton-like process with Co-Fe layered double hydroxide, *Appl. Surf. Sci.* 416 (2017) 45–50.
- [57] Y. Liu, Q. Fan, J. Wang, Zn-Fe-CNTs catalytic in situ generation of H₂O₂ for Fenton-like degradation of sulfamethoxazole, *J. Hazard Mater.* 342 (2018) 166–176.
- [58] J.Y. Cao, Z.K. Xiong, B. Lai, Effect of initial pH on the tetracycline (TC) removal by zero-valent iron: Adsorption, oxidation and reduction, *Chem. Eng. J.* 343 (2018) 492–499.
- [59] T.H. Wang, Y. Zhou, S.X. Cao, J. Lu, Y.B. Zhou, Degradation of sulfanilamide by Fenton-like reaction and optimization using response surface methodology, *Ecotox Environ. Saf.* 172 (2019) 334–340.
- [60] T. Zhou, X. Zou, J. Mao, X. Wu, Decomposition of sulfadiazine in a sonochemical Fe-catalyzed persulfate system: Parameters optimizing and interferences of wastewater matrix, *Appl. Catal. B-Environ.* 185 (2016) 31–41.
- [61] J. Kim, Y.J. Choe, S.H. Kim, K. Jeong, Enhancing the decomposition of refractory contaminants on SO₄²⁻-functionalized iron oxide to accommodate surface SO₄ center dot - generated via radical transfer from (OH)-O-center dot, *Appl. Catal. B-Environ.* 252 (2019) 62–76.
- [62] Y. Yang, X. Hu, Y. Zhao, L. Cui, Z. Huang, J. Long, J. Xu, J. Deng, C. Wu, W. Li, Decontamination of tetracycline by thiourea-dioxide-reduced magnetic graphene

- oxide: Effects of pH, ionic strength, and humic acid concentration, *J. Colloid Interface Sci.* 495 (2017) 68–77.
- [63] D. Vione, F. Merlo, V. Maurino, C. Minero, Effect of humic acids on the Fenton degradation of phenol, *Environ. Chem. Lett.* 2 (3) (2004) 129–133.
- [64] H.L. Yu, G.F. Liu, R.F. Jin, J.T. Zhou, Goethite-humic acid coprecipitate mediated Fenton-like degradation of sulfanilamide: the role of coprecipitated humic acid in accelerating Fe(III)/Fe(II) cycle and degradation efficiency, *J. Hazard Mater.* 403 (2021).
- [65] L. He, C. Yang, J. Ding, M.Y. Lu, C.X. Chen, G.Y. Wang, J.Q. Jiang, L. Ding, G.S. Liu, N.Q. Ren, S.S. Yang, Fe, N-doped carbonaceous catalyst activating periodate for micropollutant removal: Significant role of electron transfer, *Appl. Catal. B-Environ.* 303 (2022).
- [66] Z. Liu, H.J. Ding, C. Zhao, T. Wang, P. Wang, D.D. Dionysiou, Electrochemical activation of peroxydisulfate with ACF cathode: Kinetics, influencing factors, mechanism, and application potential, *Water Res* 159 (2019) 111–121.
- [67] H.L. Wang, T.H. Chen, D. Chen, X.H. Zou, M.X. Li, F.J. Huang, F.W. Sun, C. Wang, D.B. Shu, H.B. Liu, Sulfurized oolitic hematite as a heterogeneous Fenton-like catalyst for tetracycline antibiotic degradation, *Appl. Catal. B-Environ.* (2020) 260.
- [68] Y.F. Ji, Y.Y. Shi, W. Dong, X. Wen, M.D. Jiang, J.H. Lu, Thermo-activated persulfate oxidation system for tetracycline antibiotics degradation in aqueous solution, *Chem. Eng. J.* 298 (2016) 225–233.
- [69] C. Liu, H. Dai, C. Tan, Q. Pan, F. Hu, X. Peng, Photo-Fenton degradation of tetracycline over Z-scheme Fe-g-C₃N₄/Bi₂WO₆ heterojunctions: mechanism insight, degradation pathways and DFT calculation, *Appl. Catal. B-Environ.* (2022) 310.
- [70] J. Wang, D. Zhi, H. Zhou, X. He, D. Zhang, Evaluating tetracycline degradation pathway and intermediate toxicity during the electrochemical oxidation over a Ti/Ti₄O₇ anode, *Water Res* 137 (2018) 324–334.
- [71] J. Zheng, Z. Xu, S. Xin, B. Zhu, L. Nie, Generation of singlet oxygen over CeO₂/K, Na-codoped g-C₃N₄ for tetracycline hydrochloride degradation over a wide pH range, *Dalton Trans.* 51 (34) (2022) 12883–12894.
- [72] S.-W. Lv, J.-M. Liu, N. Zhao, C.-Y. Li, F.-E. Yang, Z.-H. Wang, S. Wang, MOF-derived CoFe₂O₄/Fe₂O₃ embedded in g-C₃N₄ as high-efficient Z-scheme photocatalysts for enhanced degradation of emerging organic pollutants in the presence of persulfate, *Sep. Purif. Technol.* (2020) 253.
- [73] L. Zhang, Y. Nie, C. Hu, J. Qu, Enhanced Fenton degradation of Rhodamine B over nanoscaled Cu-doped LaTiO₃ perovskite, *Appl. Catal. B-Environ.* 125 (2012) 418–424.
- [74] W.P. Kwan, B.M. Voelker, Rates of hydroxyl radical generation and organic compound oxidation in mineral-catalyzed Fenton-like systems, *Environ. Sci. Technol.* 37 (6) (2003) 1150–1158.
- [75] Y.B. Wang, H.Y. Zhao, M.F. Li, J.Q. Fan, G.H. Zhao, Magnetic ordered mesoporous copper ferrite as a heterogeneous Fenton catalyst for the degradation of imidacloprid, *Appl. Catal. B-Environ.* 147 (2014) 534–545.